Agricultural and Forest Meteorology 281 (2020) 107834

Contents lists available at ScienceDirect

Agricultural and Forest Meteorology

journal homepage: www.elsevier.com/locate/agrformet

Modeling the incoming all-wave radiation in a planted trench system

Isaac Kramer, Nurit Agam, Pedro Berliner*

The Jacob Blaustein Institutes for Desert Research, Ben-Gurion University of the Negev, Sede Boqer Campus, 8499000, Israel

ARTICLE INFO

Keywords:
Micro-catchments
Water harvesting
Radiation model
Trench orientation

ABSTRACT

Micro-catchment systems (MCs) are designed to harvest and utilize rainwater, with the aim of supporting crop growth in arid regions. While MCs were traditionally built with shallow infiltration basins, recent research indicates that MCs with deeper basins lose less water to the atmosphere than MCs with shallower basins. Consequently, we can expect more water to infiltrate the soil and be available to trees grown in deeper MCs than those grown in shallow MCs. The reduction in the direct water loss is owed, to a large extent, to the decreased flux of incoming shortwave radiation reaching the surface in deeper basins. The degree to which the incoming shortwave radiation reaching the floor of the MC is reduced, in turn, depends on the system's dimensions and orientation, geographical location, canopy geometry, soil properties, date, and time. We present a model that calculates the incoming all-wave (short- and longwave) radiation flux densities reaching any point on the floor of a trench MC in which trees are planted. To add to previously developed models that considered direct radiation, diffuse radiation, and direct and diffuse radiation reflected downwards from the walls of the trench, the model accounts for possible shading and attenuation of the radiation caused by the presence of a canopy in the system. We have also added the component of longwave radiation, considering longwave radiation emitted from the atmosphere, from the canopy of trees planted within the system, and from the trench walls.

We validated the model by comparing modeled results to field measurements inside a planted trench system. We used pyranometers to measure the incoming shortwave radiation and a 4-way net radiometer for the incoming longwave. Our results indicate that the model accurately depicts the diurnal course of shortwave and longwave radiation at different points on the floor of a N-S oriented trench MC and for different solar elevation angles. Simulations for the Negev Desert revealed that the presence of a canopy can strongly influence which trench configurations lead to the greatest decreases in incoming shortwave radiation. When a large canopy is present and the trench is wide, less radiation reaches the ground in N-S oriented trenches than in E-W oriented trenches. While the incoming longwave radiation at the bottom of the trench MC is higher than that on an equivalent horizontal surface at ground level, this increase is not enough to offset the decrease in shortwave radiation. The simulations indicate that the total incoming all-wave radiation (combined shortwave and longwave) inside trenches is less than that outside.

1. Introduction

Runoff precipitation is often the most readily available water for irrigation in arid regions. In recent years, many attempts have been made to use this resource to support plant growth (Berliner and Ben-Asher, 1994). In order to ensure survival during the long dry spells that characterize arid regions, runoff-based systems must store large volumes of water in the soil whenever a runoff event occurs.

Field trials have suggested that micro-catchments (MCs) are probably the most efficient option in terms of water supply (Berliner and Ben-Asher, 1994; Boers, 1994). MCs rely on runoff "generated from precipitation over a small catchment area" that is conveyed over a slope to an adjacent infiltration basin (Berliner and Ben-Asher, 1994; Boers, 1994). The water reaching the basin can then infiltrate into the soil, where it is stored and remains available to support tree and shrub growth during dry seasons. A MC system therefore has to be designed in such a way that the amount of runoff water collected in the depression meets the amounts transpired by the trees, accounting for losses to deep percolation and direct evaporation of water from the soil.

The reduction of the evaporative losses of water from the soil surface will increase the water available to the trees for transpiration. One possible outcome of these savings would be that if the transpiration levels are constant, the amount of runoff that has to be collected decreases. That is, the size of the runoff generating area can be decreased,

* Corresponding author.
E-mail address: berliner@bgu.ac.il (P. Berliner).

https://doi.org/10.1016/j.agrformet.2019.107834
Received 7 April 2019; Received in revised form 5 November 2019; Accepted 7 November 2019

thus increasing the potential planted area, for a given landscape. Rutten (2008) observed that evaporation pans located in the bottom of wide trenches had higher evaporation rates than those in narrow trenches and that there were differences between evaporation rates in east-west oriented pans when compared to north-south ones. Zhang et al. (2013) showed that relatively large and shallow infiltration basins result in larger evaporative losses from the soil surface, from which it follows that collection areas in the form of deep narrow trenches would be advantageous.

Finding the most efficient width to depth trench ratios requires a model that describes the process of direct evaporation of water from the surface of the wetted bottom of the trench. Evaporation of wet soils is primarily driven by the radiation flux (Baldocchi et al., 2000; Black and Kelliher, 1989; Hillel, 2003; Nyman et al., 2017; Silberstein et al., 2001) and therefore the first step in developing a comprehensive water balance model is a radiation model that will allow the estimation of incoming all-wave (combined shortwave and longwave) radiation at any point within the trench.

Experimental work using artificial trenches devoid of vegetation conformed well to a theoretical model developed in order to predict shortwave radiation fluxes reaching the bottom of trenches as a function of their geometry and geographical orientation (Agam et al., 2016). Their model estimates the total shortwave radiative flux (direct and diffuse) reaching any point on the floor of a trench including the respective fractions reflected from the walls of the trench. In order to describe the radiative fluxes within a trench system planted with trees it is necessary to modify and extend the Agam et al. (2016) model to account for the interception of direct and diffuse radiation by the canopies and the fluxes of the incoming longwave radiation from the sky and from the canopy.

The model of Zhao et al. (2003) allows the computation of radiation fluxes at any point on the soil surface, between trees and on the edges of orchards, for any canopy configuration, and is therefore well suited to serve our needs. Techniques used to model the incoming longwave radiation underneath a canopy have been developed (Black et al., 1991; Essery et al., 2008; Lu et al., 2014; Oke, 2002; Pomeroy et al., 2009) and particularly the model presented by Essery et al. (2008) can be adapted to our case in order to explicitly assess the flux of incoming longwave radiation at the trench floor. Our goal was to develop a radiation model that allows the computation of incoming all-wave radiation at any point on the bottom of a trench, taking into account trench geometry (i.e., depth, width and geographical orientation) and albedo, canopy geometry (spacing between trees, canopy height and radius and the optical properties of the canopy), and differences in site location (latitude, longitude).

Water scarcity and the probable change in rainfall patterns in drylands due to global climate change (IPCC, 2007) will increase the need to efficiently use all available water sources, runoff being one of the most readily available ones (Berliner and Ben-Asher, 1994). Runoff water has to be collected in plots or trenches and experimental evidence indicates that the latter is preferable (Leake, 2015). The fact that there are a very large number of possible combinations of canopy size, canopy structure and trench geometry (depth/width ratio and orientation), together with the time and cost required to select the combination that minimizes direct evaporative losses, makes the use of a model almost mandatory. There are no such models available and bearing in mind that radiation is the main driver for water evaporation from soils, the first step towards such a model is to consider all the radiative fluxes at the bottom of a trench.

2. Model description

2.1. Incoming shortwave radiation overview

The model considers four separate sources when calculating the total incoming shortwave radiation ($\downarrow SR$) reaching the floor of a trench micro-catchment (TMC): direct solar radiation (S_D), diffuse solar radiation emanating from the celestial hemisphere (Ω_D), and reflected direct (S_R) and diffuse radiation (Ω_R) from the trench walls, each component is measured in W m^{-2} The total incoming shortwave radiation reaching a point on the trench floor is then:

$$\downarrow SR = S_D + \Omega_D + S_R + \Omega_R \tag{1}$$

The magnitude of each of these components depends upon the properties of the TMC, including its geographical location and orientation, as well as on those of the canopy of the trees planted within the TMC.

2.1.1. Direct shortwave radiation

Wall shading If a given point on the trench floor is shaded by the trench's walls, no direct shortwave radiation will reach this point. If the point is not shaded, then the flux of direct shortwave radiation will not be affected by the trench walls. To determine whether a given point on the trench floor is shaded by the trench wall, we followed Agam et al. (2016), as detailed in Appendix A.

Canopy shading When a point on the floor of TMC is not shaded by the walls, the flux of direct radiation it receives can either be equal to that measured on a horizontal surface outside the trench, or it can be shaded by the canopy of trees planted within the system. To describe the degree of attenuation of incoming shortwave radiation by the canopy, the model uses Beer's Law, as in Zhao et al. (2003):

$$I = I_0 e^{-kx} \tag{2}$$

where

I_0	intensity of the radiation (W m^{-2})
I	intensity of the radiation after passing through the canopy (W m^{-2})
x	depth of canopy a beam of radiation passes through (m)
k	extinction coefficient (based on the canopy's opacity, m^{-1})

Calculating the canopy depth. The canopy depth (x) for a given point, m, depends on that point's position relative to the canopy and the position of the sun. We assume a spherical-shaped canopy. Spherical canopies are common in agroforestry systems (Zhao et al., 2003). To calculate x for a tree with height H (height from ground to center of canopy, m), canopy radius r (m), and where the distance from the base of the tree and to m is p, we modify the method presented by Zhao et al. (2003) and define the angles ϑ, δ, and ω, as shown in Fig. 1. We also define φ and ϕ as the elevation and azimuth angles, respectively, as shown in Fig. 3.

If $\vartheta \geq \delta$, the incoming solar radiation does not pass through the canopy and m is not shaded by the canopy. If $\vartheta < \delta$, then it is possible that m is shaded by the canopy. This, along with the calculation of the canopy depth, $x(\vartheta)$, are described as follows:

$$H = OE \tag{3}$$

$$mO = \sqrt{H^2 + p^2} \tag{4}$$

$$mA = \sqrt{H^2 + p^2 - r^2} \tag{5}$$

$$\tan\omega = \frac{H}{p} \tag{6}$$

$$\tan\delta = \frac{r}{\sqrt{H^2 + p^2 - r^2}} \tag{7}$$

$$BC = \begin{cases} \sqrt{OC^2 - OB^2} = \sqrt{r^2 - (H^2 + p^2)\sin^2\vartheta} & \text{if} \varphi < \delta \\ 0 & \text{if} \vartheta \geq \delta \end{cases} \tag{8}$$

$$x(\vartheta) = CD = \begin{cases} 2\sqrt{r^2 - (H^2 + p^2)\sin^2\vartheta} & \text{if} \varphi < \delta \\ 0 & \text{if} \vartheta \geq \delta \end{cases} \tag{9}$$

In order to calculate the values of ϑ, δ, ω, and p and thereby $x(\vartheta)$, it

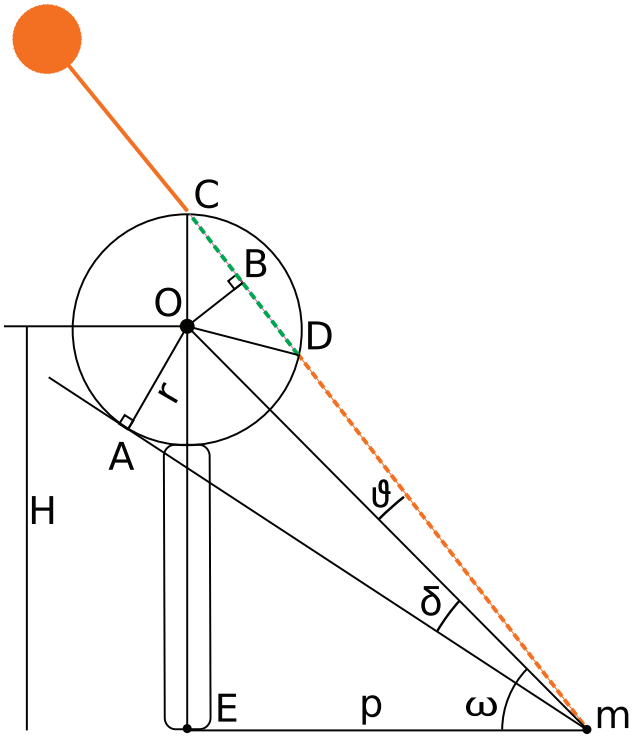

Fig. 1. The canopy depth a beam of radiation directed towards point *m* on the ground must penetrate while passing through a single tree with a spherical crown.

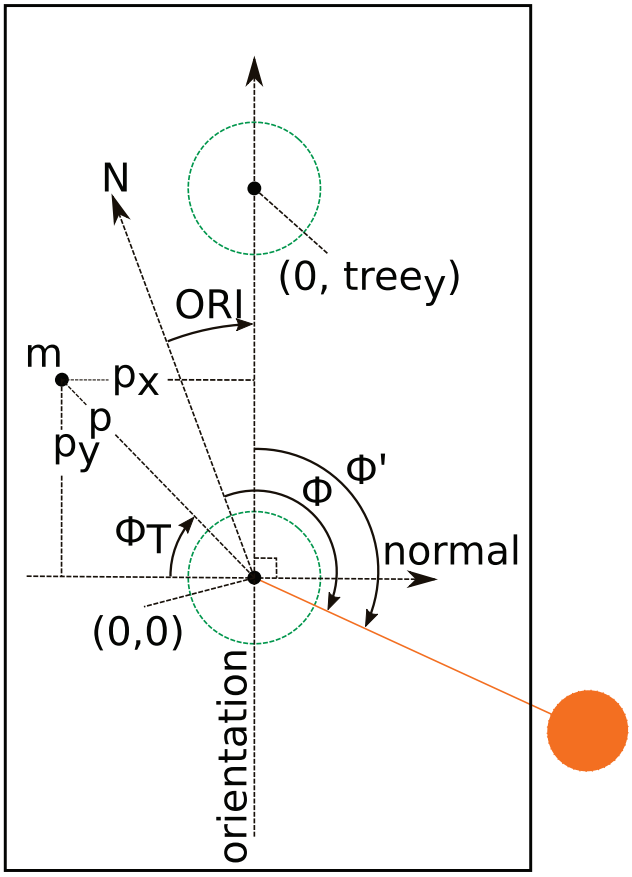

Fig. 2. The coordinate system used to calculate the canopy depth for any point *m* on the floor of a TMC.

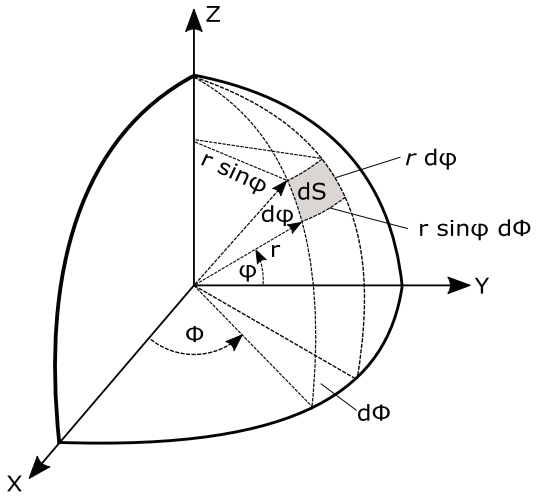

Fig. 3. The differential area (d*S*) on the celestial hemisphere.

is necessary to introduce a coordinate system connecting the position of point *m* to the trees inside the trench (Fig. 2). We achieve this by defining:

- the tree nearest to point *m* as the origin.
- the orientation angle of the trench with respect to north (*ORI*) as the y-axis and the normal to this as the *x*-axis.

The location of any point *m* can then be re-expressed in relation to the tree as $p(p_x, p_y)$, where p_x and p_y are the distance from the tree relative to the *x*-axis and *y*-axis respectively. We further define ϕ' as the azimuth angle of the sun relative to the *ORI*:

$$\phi' = \phi - ORI \tag{10}$$

and ϕ_T as the azimuth angle of the tree relative to the normal:

$$\phi_T = \arctan \frac{p_x - tree_x}{p_y - tree_y} \tag{11}$$

where $tree_x$ and $tree_y$ define the location of a tree within the coordinate system. The value ϑ is then given by:

$$\cos\vartheta = \sin\varphi \sin\omega + \cos\varphi \cos\omega \cos(\phi' - \phi_T) \tag{12}$$

Therefore, combining Eqs. (10) and (12) yields:

$$\sin^2\vartheta = 1 - \cos^2\vartheta = 1 - [\sin\varphi \sin\omega + \cos\varphi \cos\omega \cos(\phi - \phi_T - ORI)]^2 \tag{13}$$

The canopy depth for any tree in the trench system can then be reformulated as:

$$x_{i,j}(\varphi, \phi) = 2\sqrt{r^2 - [H^2 + (p_x)^2 + (p_y)^2]\sin^2\vartheta} \tag{14}$$

This system can easily be extended to calculate the canopy depth for multiple trees, as additional trees can be defined using the same coordinate system. In this case, *x* is defined as the sum of the canopy depth in the direction (φ, ϕ) and is given by:

$$x(\varphi, \phi) = \sum_{i=1}^{n} x_i(\varphi, \phi) \tag{15}$$

where x_i is a given tree and *n* is the number of trees inside the trench system. The model only considers shading from trees within a single trench system (i.e., the possibility of shading from trees in other trench systems is ignored).

Calculating the extinction coefficient. The method used to describe calculation of the extinction coefficient is described in detail in Section 3.1.

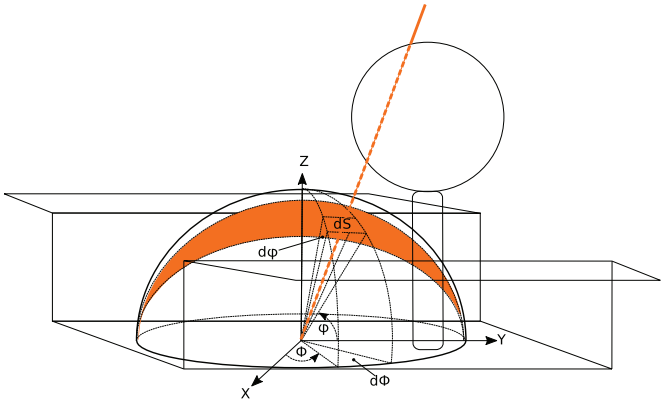

Fig. 4. The diffuse radiation reaching the floor of a TMC is obstructed by the trench walls and the presence of a canopy.

2.1.2. Diffuse shortwave radiation

Assuming the diffuse radiation is isotropic, the total diffuse radiation reaching a horizontal surface outside the trench could be found by integrating over the celestial hemisphere. To integrate the diffuse radiation over the hemisphere, the differential surface area of the hemisphere (dS) is defined as (Fig. 3) (Agam et al., 2016; Zhao et al., 2003):

$$\mathrm{d}S = r^2 \cos\varphi \mathrm{d}\varphi \mathrm{d}\phi \tag{16}$$

The diffuse radiation emanating from dS and directed to a given point (m) is then:

$$\Omega_m = \Omega_{\mathrm{d}S} \sin\varphi \mathrm{d}S = \Omega_{\mathrm{d}S}\ r^2 \cos\varphi \mathrm{d}\varphi \mathrm{d}\phi \tag{17}$$

The diffuse radiation reaching points on the trench floor, however, is restricted by the trench's walls and presence of the canopy (Fig. 4).

The fraction of diffuse radiation that is visible at a given point is based on the meridional view angles for that point on the trench floor, ε_1 and ε_2 (Fig. 5), which are defined such that:

$$\varepsilon_1 = \arctan\frac{D}{m_x} \tag{18}$$

and

$$\varepsilon_2 = \arctan\frac{D}{W - m_x} \tag{19}$$

where m_x is the distance between point m and WALL 1.

As with direct radiation, the model applies Beer's Law (Eq. (2)) to estimate the attenuation of diffuse radiation passing through the canopy, considering the entire visible portion of the celestial hemisphere.

The diffuse radiation reaching point m on the floor of a TMC is thus expressed as follows:

$$\Omega_m = \Omega_{\mathrm{d}S}\ r^2 \int_0^{2\pi}\int_{\varepsilon_1}^{\varepsilon_2} \mathrm{e}^{-kx(\varphi,\phi)} \sin\varphi\cos\varphi \mathrm{d}\varphi\mathrm{d}\phi \tag{20}$$

We define c as a point at which the same fraction of the celestial hemisphere is visible as at point m, but at which no radiation is obstructed by the canopy. The diffuse radiation reaching point c can be defined as

$$\Omega_c = \Omega_{\mathrm{d}S}\ r^2 \int_0^{2\pi}\int_{\varepsilon_1}^{\varepsilon_2} \sin\varphi\cos\varphi \mathrm{d}\varphi\mathrm{d}\phi \tag{21}$$

Reordering this integral to consider the orientation of the trench yields:

$$\Omega_c = \Omega_{\mathrm{d}S}\ r^2 \int_{ORI}^{ORI+2\pi}\int_{\varepsilon_1}^{\varepsilon_2} \sin\varphi\cos\varphi \mathrm{d}\varphi\mathrm{d}\phi \tag{22}$$

which can be rewritten:

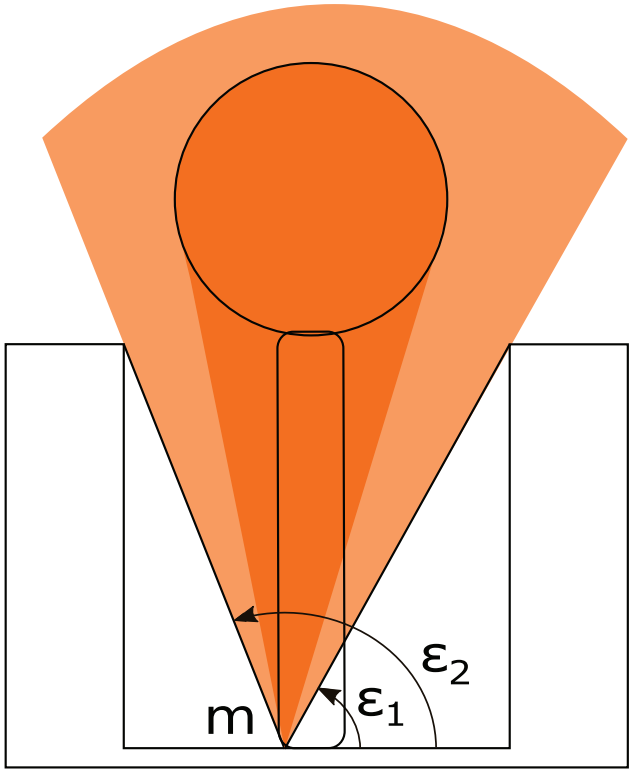

Fig. 5. The meridional angles ε_1 and ε_2 which are used to calculate the fraction of the diffuse radiation reaching points on the floor of a TMC.

$$\Omega_c = \Omega_{\mathrm{d}S}\ r^2 \int_{ORI}^{ORI+\pi}\int_{\varepsilon_1}^{\pi/2} \sin\varphi\cos\varphi \mathrm{d}\varphi\mathrm{d}\phi + \Omega_{\mathrm{d}S}\ r^2 \int_{ORI+\pi}^{ORI+2\pi}\int_{\varepsilon_2}^{\pi/2} \sin\varphi\cos\varphi \mathrm{d}\varphi\mathrm{d}\phi \tag{23}$$

With the solution to the integral then:

$$\Omega_c = \Omega_{\mathrm{d}S}\ r^2\pi(\cos^2\varepsilon_1 + \cos^2\varepsilon_2) \tag{24}$$

and we can therefore rewrite Eq. (22):

$$\Omega_m = \frac{\Omega_c}{\pi(\cos^2\varepsilon_1 + \cos^2\varepsilon_2)} \int_{ORI}^{ORI+2\pi}\int_{\varepsilon_1}^{\varepsilon_2} \mathrm{e}^{-kx(\varphi,\phi)} \sin\varphi\cos\varphi \mathrm{d}\varphi\mathrm{d}\phi \tag{25}$$

It remains, therefore, to solve for Ω_c. Eq. (22) can be solved such that:

$$\Omega_c = \frac{1}{2}\Omega_{\mathrm{d}S}\ r^2\pi[\cos\varepsilon_1 - \cos\varepsilon_2] \tag{26}$$

Normalizing Ω_c based on the total diffuse radiation outside a trench system (Ω_a), we can write:

$$\Omega_c = \Omega_a \frac{1}{2}[\cos\varepsilon_1 - \cos\varepsilon_2] \tag{27}$$

The total diffuse radiation at point m inside the trench system can therefore be written as:

$$\Omega_m = f_{tc}\Omega_a \tag{28}$$

where f_{tc} is the fraction of the diffuse radiation outside the trench system that reaches point m inside the trench, also considering the presence of a canopy, and is given by:

$$f_{tc} = \frac{[\cos\varepsilon_1 - \cos\varepsilon_2]}{2\pi(\cos^2\varepsilon_1 + \cos^2\varepsilon_2)} \int_{ORI}^{ORI+2\pi}\int_{\varepsilon_1}^{\varepsilon_2} \mathrm{e}^{-kx(\varphi,\phi)} \sin\varphi\cos\varphi \mathrm{d}\varphi\mathrm{d}\phi \tag{29}$$

2.1.3. Reflected direct shortwave radiation

To model the reflected direct radiation, we follow the model presented by Agam et al. (2016), as described in Appendix B.

If the direct radiation passes through the region of the canopy prior to reaching the trench wall, its intensity will be reduced. To account for this reduction, the model redefines the direct solar radiation reaching the wall of the trench (S_W), such that:

$$S_W = \int_0^{\pi} \int_{\varepsilon_4}^{\varepsilon_3} S_W \, e^{-kx(\varphi,\phi)} d\varphi d\phi \tag{30}$$

where, in this case, φ and ϕ define the portion of the celestial hemisphere, as seen from point m, from which reflected radiation may be directed. The angles ε_3 and ε_4 are defined in Fig. B.5.

2.1.4. Reflected diffuse shortwave radiation

The reflected diffuse radiation model procedure (following Agam et al. (2016)) is described in Appendix C.

The presence of a canopy can result in the attenuation of the diffuse radiation reaching the trench's wall, and thus modify the diffuse radiation reaching the trench's walls (Ω_W). As with the diffuse radiation in Section 2.1.2, the change in the value of the diffuse radiation reaching point i can be accounted for by applying Beer's Law (Eq. (2)), and integrating over the visible portion of the celestial hemisphere, such that for points on WALL 1, where γ_i is defined in Eq. (C.2):

$$\Omega_{W-i} = \Omega_a f_i \frac{1}{\pi \cos^2 \gamma_i} \int_{ORI+\pi}^{ORI+2\pi} \int_{\pi/2-\gamma_i}^{\pi/2} e^{-kx(\varphi,\phi)} d\varphi d\phi \tag{31}$$

and for points on WALL 2:

$$\Omega_{W-i} = \Omega_a f_i \frac{1}{\pi \cos^2 \gamma_i} \int_{ORI}^{ORI+\pi} \int_{\pi/2-\gamma_i}^{\pi/2} e^{-kx(\varphi,\phi)} d\varphi d\phi \tag{32}$$

We account for the variation in Ω_{W-i} over the length of the trench wall by integrating over the portion of the wall seen from point m, such that for points on WALL 1:

$$\Omega_W = \int_0^{\pi} \int_0^{\varepsilon_5} \Omega_{W-i} d\varphi d\phi \tag{33}$$

and for points on WALL 2:

$$\Omega_W = \int_0^{\pi} \int_0^{\varepsilon_6} \Omega_{W-i} d\varphi d\phi \tag{34}$$

where ε_5 and ε_6 are defined in Eqs. (C.6) and (C.7), respectively.

2.2. Incoming longwave radiation

To model the incoming longwave radiation reaching the floor of a TMC, we separately consider the flux of longwave radiation emitted from the visible portion of the sky above the trench and that emitted from the trench walls. In the case of the former, the model considers longwave radiation emitted by the canopy and the unobstructed sky above the trench. The three sources of incoming longwave radiation are shown in Fig. 6. Each component is measured in W m^{-2}.

The flux of radiation emitted from any body (LR) is given by $LR = \varepsilon_s \sigma T_s^4$ where ε_s is the emissivity of the object, σ is the Stefan-Boltzmann constant, and T_s is the temperature of the emitting body (K). The model applies this law to each of the sources in question.

2.2.1. Longwave radiation emitted from above the trench

Because the longwave radiation emanating from the celestial hemisphere above the trench may be obstructed by the canopy, the model must first consider what fraction of the celestial hemisphere is occupied by the canopy. The total incoming longwave radiation from the celestial hemisphere above the trench (LR_{hem}) can then be written:

$$LR_{hem} = p_c LR_{air} + (1 - p_c) LR_{canopy} \tag{35}$$

where LR_{air} is the longwave radiation emitted by the air, LR_{canopy} is the longwave radiation emitted by the canopy, and p_c is the proportion of the hemisphere obstructed by the canopy (Pomeroy et al., 2009). The value of p_c can be found by using methods similar to that used to calculate the diffuse shortwave radiation, as in Section 2.1.2. In that case

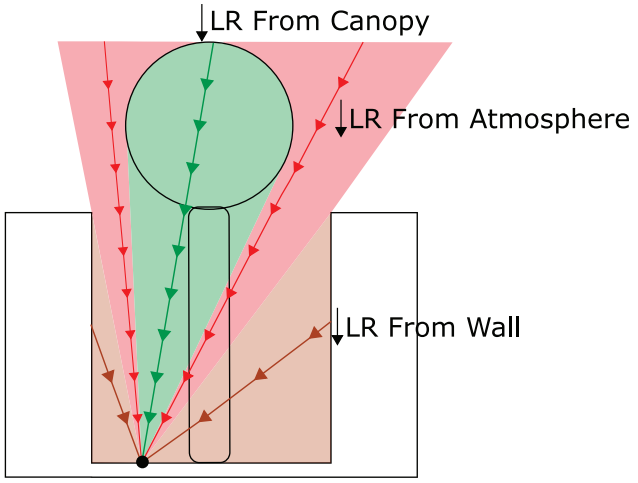

Fig. 6. Figure showing the three sources of longwave radiation (LR) reaching a point on the floor of the trench: the trench walls, the atmosphere above the trench, and the canopy above the trench.

we calculated the canopy depth for each potential combination of elevation and azimuth angles. Here, however, we simply need the fraction, p_c, of the celestial hemisphere occluded by the canopy. The value of p_c can be calculated from:

$$p_c = \frac{1}{2\pi} \int_0^{\pi/2} \int_0^{2\pi} \sin 2\varphi c(\varphi, \phi) d\phi d\varphi \tag{36}$$

where $c(\varphi, \phi) = 1$ if not occluded by the canopy and 0 otherwise. We implicitly assume that only in this case that the canopy is opaque and gapless. This assumption will not lead to a significant error in the total longwave radiation reaching a specific point on the bottom of the trench. The gap frequency is usually low and the difference between the longwave radiation flux that is emitted by the canopy and the flux that would pass through a gap is proportional to the difference between the emissivity of the atmosphere and that of the canopy.

Longwave radiation emitted from the atmosphere The atmospheric emissivity coefficient (ε_a) can be calculated as an empirical function of the air's temperature and water vapor pressure (Brutsaert, 2013):

$$\varepsilon_a = 1.24 \left(\frac{e_a}{T_a}\right)^{\frac{1}{7}} \tag{37}$$

where T_a is the temperature of the air (K) and e_a (mbar) is the partial water vapor pressure of the air. e_a is itself a function of the relative humidity (RH) and the saturation vapor pressure (e_{sat}, mbar) at air temperature and approximated by using (Brutsaert, 2013):

$$e_a = RH \cdot e_{sat} \tag{38}$$

where e_{sat} is calculated (Brutsaert, 2013):

$$e_{sat} = 6.11 e^{\frac{17.4 T_a}{239 + T_a}} \tag{39}$$

Longwave radiation emitted from the canopy

To calculate the longwave radiation emitted from the canopy, we must likewise have the emissivity coefficient of the canopy. The canopy emissivity (ε_c) for most trees is typically between 0.97 and 0.98 (Oke, 2002). As the longwave radiation directed towards the trench floor is from the bottom-facing side of the canopy, the model assumes that the temperature of the emitting leaves is equal to air temperature (Black et al., 1991; Pomeroy et al., 2009). In modeling the longwave radiation, we also assume that the canopy is gapless.

The total incoming longwave radiation from the region above the trench can therefore be modeled by:

$$LR_{hem} = p_c \varepsilon_c \sigma T_a^4 + (1 - p_c) \varepsilon_a \sigma T_a^4 \tag{40}$$

2.2.2. Longwave radiation emitted from the trench walls

The longwave radiation emitted from a point on the trench wall (LR_W) is dependent on the wall's temperature and its emissivity:

$$LR_W = \varepsilon_W \sigma T_W^4 \tag{41}$$

where ε_W is the emissivity of the wall and T_W is the temperature of the wall (K). We assume that the temperature of the wall is equal to the temperature of the dry soil surface (T_s) when the wall is sunlit and equal to the air temperature if the wall is shaded. To determine if a given trench wall is shaded, we apply the equations used in Section 2.1.1.

The longwave radiation emitted by the trench walls and reaching a given point on the trench floor can be computed similarly to the reflected diffuse radiation, except in this case we assume that the flux of longwave radiation is equal at all points on a given wall's height and length. We make this assumption because the affect of canopy shading on the trench walls is likely to be minimal. The longwave radiation reaching a given point on the trench floor is then given by:

$$LR_{wall} = \varepsilon_W \sigma T_W^4 \left(1 - \frac{(\cos \varepsilon_5 + \cos \varepsilon_6)}{2}\right) \tag{42}$$

where $\cos \varepsilon_5$ and $\cos \varepsilon_6$ are used to find the fraction of the LR_W directed towards a given point on the floor, and are defined as in Fig. C.7.

2.2.3. Total longwave radiation

The total longwave radiation reaching a point on the floor of a TMC can then be written:

$$LR_{TMC} = LR_{hem} + LR_{Wall} = p_c T_a \varepsilon_c + (1 - p_c) T_a \varepsilon_a + \varepsilon_W \sigma T_s^4 \left(1 - \frac{(\cos \varepsilon_5 + \cos \varepsilon_6)}{2}\right) \tag{43}$$

3. Materials and methods

Validation of the model was carried out at the Blaustein Institutes for Desert Research, Ben-Gurion University of the Negev. The campus is located in Sede Boqer, Israel (30.855375°N, 34.780739°E,400 m AMSL). At this site, there are several TMCs with trees planted inside them. Each of these trenches is approximately 12 m long, 1 m wide, and 1 m deep. They are aligned − 10° from north. Three olive trees (*Olea europaeacar Barnea*) were planted in each trench in 2010. The base of each tree is located near the axis of the trench, and the trees are spaced at 4 m intervals.

3.1. Shortwave radiation measurements

The shortwave radiation model was validated using measurements from April – June 2017. During this time, pyranometers (CM5 and CM6B, Kipp & Zonen, B.V. Delft, The Netherlands) were placed at several points on the bottom of a single TMC and used to measure the incoming shortwave radiation. Variations in measurement location and time of year allowed us to test the model's response to different combinations of canopy and wall shading and different solar elevation angles. The location of the points and the dates they were measured are presented in Figure Fig. 7. Table 1 lists the exact location of the points with respect to the trench's walls and the trees planted inside the trench. Because the TMC was nearly north-south oriented, almost none of the canopy shading fell in the region to the south of each respective tree. To best evaluate the model's ability to predict the effects of both canopy and wall shading, the majority of the pyranometers were placed in the region immediately to the north of one of the trees. Prior to the measurement period, the pyranometers were calibrated against measurements from the Ben-Gurion National Solar Energy Center (BGNSEC). Output from the pyranometers was measured and recorded at one minute intervals (CR1000 datalogger, Campbell Scientific Ltd., Logan, UT, USA).

The average canopy radius was calculated by measuring the diameter in several directions. Because the height of the trench's eastern wall was slightly higher than the western wall, we introduced separate wall heights when running the model. The height of the eastern wall was 0.9 m and that of the western wall 0.75 m. The total length of the trench was 12.0m. The height, radius, and relative positions of the trees are given in Table 2.

The extinction coefficient of a given tree is governed by the density of the canopy and its leaf properties. Previous work has shown that the extinction coefficient can be calculated from the leaf area index (LAI) and the leaf inclination distribution (Duursma et al., 2003). Measuring the LAI, however, is complicated and time consuming (Jonckheere et al., 2004; Macfarlane et al., 2007; Saitoh et al., 2012).

To estimate the extinction coefficient, we used two pyranometers: one shaded by a tree inside the trench and one on a horizontal surface outside. By comparing the direct shortwave radiation passing through the canopy to that measured outside, along with a corresponding measured value of the canopy depth, we were able to estimate the

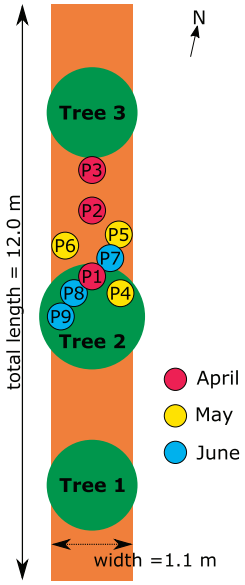

Fig. 7. Arrangement of the pyranometers during the shortwave validation.

Table 1
The coordinates of each pyranometer with respect to the trench's eastern wall (widthwise) and TREE 2 (lengthwise) during the shortwave validation.

Point	Width (m)	Length (m)	Phase
1	0.6	0.55	Apr.
2	0.6	1.45	Apr.
3	0.6	3.55	Apr.
4	0.1	0.4	May
5	0.1	1.3	May
6	1.0	1.25	May
7	0.3	0.85	June
8	0.7	0.35	June
9	1.0	0.0	June

Table 2
Height, radius, and relative position of the trees in the TMC during the validation period.

	Height (m)	Radius (m)	From southern edge (m)
Tree 1	2.75	0.94	1.70
Tree 2	2.70	0.83	5.30
Tree 3	2.3	0.62	9.65

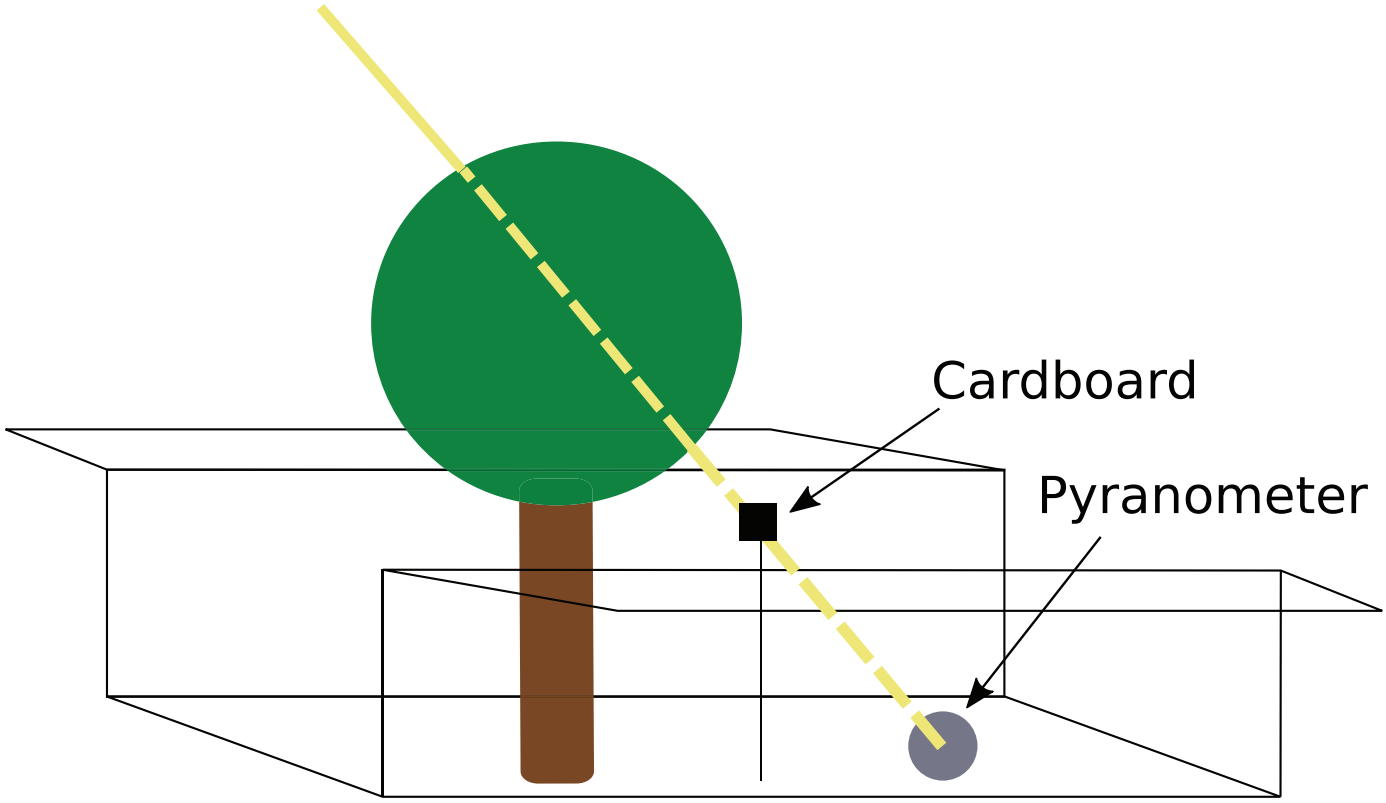

Fig. 8. Pyranometers and small pieces of cardboard were used to measure the extinction coefficient.

extinction coefficient by solving for k:

$$S_{C=}S_0 e^{-kx} \tag{44}$$

where S_C is the direct radiation passing through the canopy, S_0 is the direct radiation measured outside the trench, and x is the measured canopy depth.

To measure S_C and S_0 we successively (i) fully exposed both pyranometers for five minutes and (ii) shaded both so that all direct radiation was obstructed for five minutes. The shading was accomplished using similarly sized small elements located at the same azimuth and elevation (corresponding to that of the sun) and at a distance of 1 m from the respective pyranometers (Fig. 8). Subtracting the latter from the former for each pyranometer yields the direct solar radiation impinging on each of them.

In shading the pyranometer, we also blocked a small fraction of the diffuse radiation. The small solid angle occluded by the shade should not practically affect the absolute computation of the diffuse or direct radiation and even less the ratio of both because the shading element was similar and occluded the same solid angle.

Responses for the first minute of each repetition were removed before analysis, to account for any possible lag in the pyranometer readings. The measurements were taken at the time when the sun was directly aligned with the trench (i.e., when the azimuth angle of the sun was 170°), so that the shadow produced by the canopy was directly aligned with the center of the trench. The test was repeated three times during the year to account for possible effects of solar elevation angle.

The values of S_C and S_0 needed to solve Eq. (44) were obtained using:

$$S_C = G_T - D_C \tag{45}$$

$$S_0 = G_0 - D_0 \tag{46}$$

where $_C$ and $_0$ correspond to the values measured with canopy and without canopy, respectively. We then solved Eq. (44) such that

$$k = \frac{\ln(\frac{S_T}{S_0})}{-x} \tag{47}$$

No significant variation in the value of k was observed between the different measurements. In running the model, we used the average value from all measurements, which was found to be 1.05 m^{-1}.

The albedo of the trench walls was taken to be 0.42, derived from measurements of incoming and reflected radiation components made with a CNR1 4-way net radiometer (Kipp & Zonen, Holland) installed approximately 400 m from the field site at a height of 2.5 m. As inputs for the measured diffuse and direct radiation outside the trench, we used data provided by the BGNSEC.

3.2. Longwave radiation measurements

Validation of the longwave radiation model was conducted in June 2017. At this time, a 4-component net radiometer measuring incoming and outgoing short- and longwave radiation was placed on the floor of the same TMC used for the shortwave validation. The net radiometer was placed in the region between the second and third tree (from south). The location of the points and the dates in which they were measured are presented in Fig. 9. Fig. 9 lists the coordinates of these points with respect to the trench's walls and the trees planted within the trench.

The emissivity of the soil surface was taken as 0.963, as measured by Jiang (2016) for a similar soil. Based on values from the literature, we assumed a leaf emissivity of 0.98 (Oke, 2002; Pomeroy et al., 2009).

To compare our measurements of the longwave radiation inside the TMC to that outside the trench, we calibrated the net radiometer against the expected longwave radiation, calculated using the method described in Section 2.2.1, where inputs for relative humidity, soil temperature, and air temperature were obtained from our longterm onsite meteorological measurements.

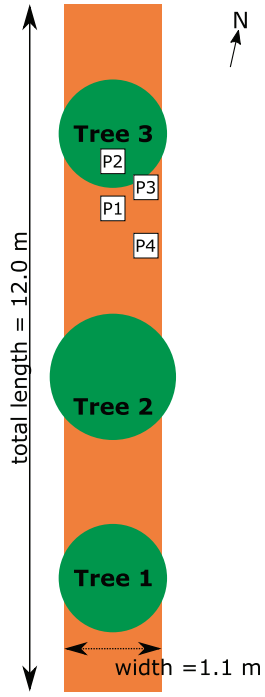

Fig. 9. The arrangement of the net-radiometer during the longwave validation.

4. Results

4.1. Shortwave radiation validation

Measurements from five cloudless days in each of April, May, and June were used to assess the fitness of the model. Plots showing the diurnal course of the measured and modeled shortwave radiation (1-hour averages) are included in Fig. 10. The plots correspond to data from a single representative day during each of the three months. The plots also include the global shortwave radiation, i.e., the total direct and diffuse radiation measured on a horizontal surface outside the trench (Brutsaert, 2013). Table 4 compares the daily total of the measured and modeled incoming shortwave radiation (MJ m^{-2} d^{-1}) at each of the respective measured positions during these single day periods. All results are based on 1-hour time-averaged measured and modeled values. The diurnal trends and integrated totals were nearly identical for other cloudless days during the measurement period.

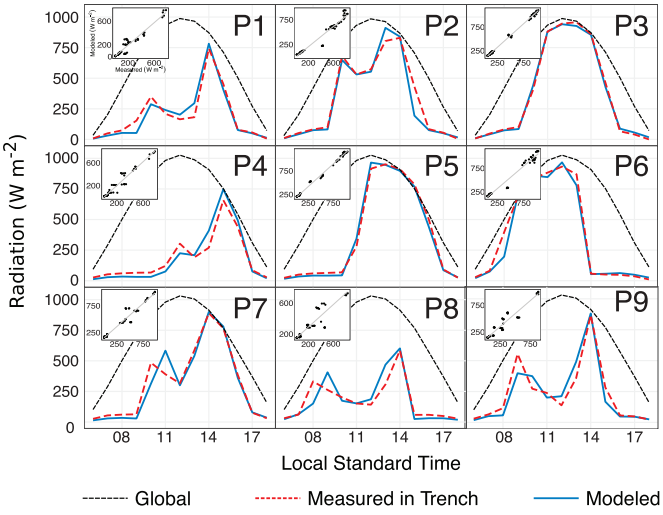

Fig. 10. Plots comparing the modeled and measured incoming shortwave radiation inside the trench. Data corresponds to a single cloudless day in each of April (P1-P3), May (P4-P6), and June (P7-P9). The inserts are modeled (y-axis) vs. measured (x-axis).

A satisfactory agreement is observed between the measured and modeled results at each of the selected points. For each of the evaluated points, the difference between the measured and modeled totals is less than 5% of the measured value. The largest percent errors are seen for POINT 2 and POINT 6. Even here, however, the difference between the modeled and measured values was less than 3% of the global shortwave radiation on that day.

Data from all five cloudless days during each of the three measurement periods were used to linearly correlate the measured vs. modeled results (Fig. 10). Statistical summaries of the linear regression models are presented in Table 4. In all but two cases, the intercepts were not significant. The R^2 values were greater than 0.9 in all but one case and greater than 0.95 for five of the nine.

Some divergence between the modeled and measured radiation is, however, observed. The model significantly underestimates the incoming shortwave radiation at certain times, such as POINT 1 at 09:00, POINT 2 at 15:00, POINT 6 at 08:00, and POINT 7 at 15:00. These differences are likely caused by imperfections in the trench construction. Specifically, because of small dips along the lip of the trench, the trench's width and depth are not perfectly consistent. At these points, the trench wall is either slightly shorter or its width is slightly wider than the average value, thereby causing the actual incoming shortwave radiation to be greater than that anticipated by the model. Examination of the errors by time of day (Fig. 11, data from all five days in each of the measurement periods) shows that the model consistently underestimates the incoming shortwave radiation at all points during the morning hours. We argue that these differences stem from the imperfections in the trench construction rather than from misrepresentation of the model. Because the trench wall was not completely perpendicular, the model is prone to underestimating the incoming direct shortwave radiation and also the reflected radiation and diffuse components.

Fig. 10 shows that the model often produces errors in estimating the degree to which a given point is shaded or not shaded by the canopy. This is most likely caused by the canopy not being perfectly spherical and its leaf distribution not being strictly homogeneous. The relative errors, however, are small and overall the model's results fit the measured values.

4.2. Longwave radiation validation

For each of the four measurement points, data from a single cloudless day in June urntOrangewere used to assess the fitness of the model. Plots showing the diurnal course of the measured and modeled longwave radiation (1-hour averages) at each of the points are shown in Fig. 12. In all cases, the measured and modeled longwave radiation inside the trench is greater than that measured outside the trench. While only a fraction of the celestial hemisphere is visible to points inside the trench, thereby limiting incoming longwave radiation from the atmosphere, the total flux of longwave radiation reaching the trench floor is higher than that outside the trench because points on the trench floor also receive longwave radiation emitted by the trench walls.

Table 5 compares the integrated total (MJ m^{-2} d^{-1}) for the measured and modeled incoming longwave radiation at each of the respective points. The data used to compute the integrated totals corresponds to the same cloudless days plotted in Fig. 12. The errors are less than 5% for each of the points.

Data from each of the points were used to linearly correlate the measured vs. modeled results (Fig. 12). Statistical summaries of the linear models are presented in Table 5. While the models show high R^2 values (greater than 0.87 in all cases), the values of the intercepts are significant and the slopes are noticeably different from 1 for three of the four points. Examination of the plots shows that this is likely due to a level of hysteresis due to the assumptions introduced regarding the

Table 4
Comparison of the measured and modeled daily totals for incoming shortwave radiation inside the TMC on representative single days. Data corresponds to a single cloudless day in each of April (P1-P3), May (P4-P6), and June (P7-P9).

Point	Measured	Modeled	Abs. Diff.	Error	Linear Regression				
	MJ m^{-2} d^{-1}	MJ m^{-2} d^{-1}	MJ m^{-2} d^{-1}	Percent	Slope	Intercept	R^2	Standard Error (W m^{-2})	MAE (W m^{-2})
1	9.14	8.98	0.16	1.8	*0.95*	-0.26	0.93	53.4	39.6
2	15.24	14.5	0.74	4.9	*0.99*	-17.70	0.95	72.4	37.7
3	17.50	17.44	0.06	0.3	0.96	8.89**	0.99	22.3	21.1
4	8.52	8.61	0.09	-1.1	1.14	-21.04**	0.95	49.9	40.3
5	16.75	17.02	0.27	-1.6	*1.00*	-4.73*	0.99	30.5	21.8
6	17.95	17.0	0.95	5.3	0.96	-11.48	0.98	57.5	36.3
7	15.07	14.40	0.47	3.1	*0.98*	-11.65	0.94	72.3	41.8
8	8.14	8.39	0.25	-3.0	*1.07*	-7.91	0.82	77.9	52.2
9	10.85	10.69	0.27	2.5	*0.98*	2.33	0.91	70.6	51.6

MAE is mean absolute error. * $p < .1$; ** $p < .05$; *** $p < .01$. Slopes not significantly different than one are italicized ($p < .05$).

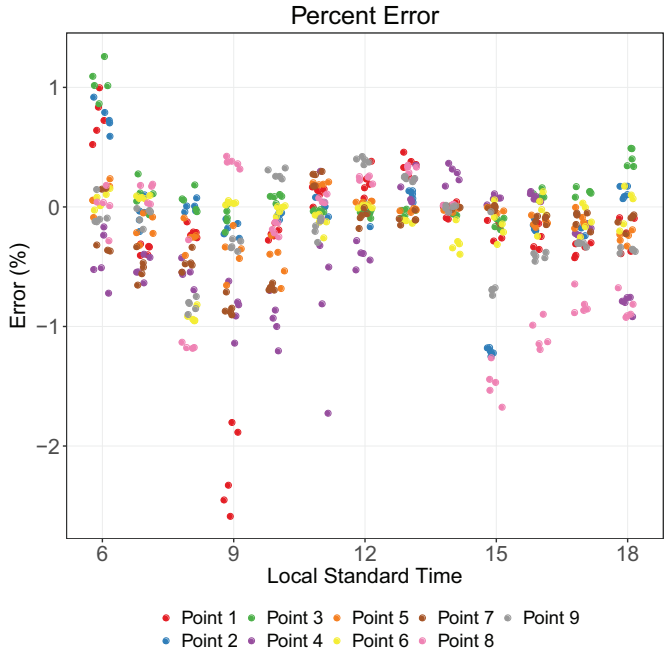

Fig. 11. Percent error at each of the nine points during the validation of the shortwave model. Data from all five days in each respective measurement period.

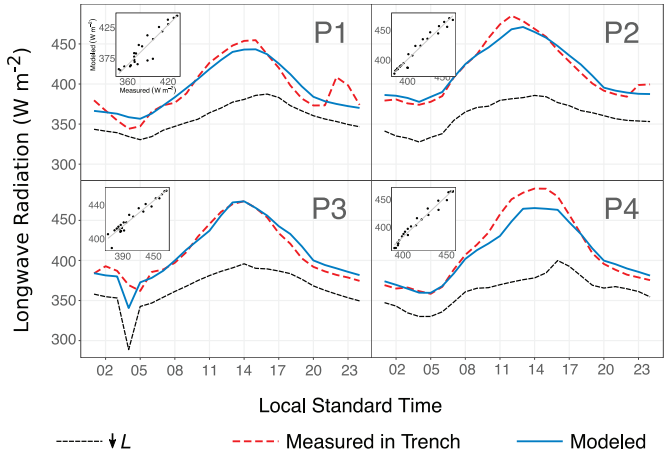

Fig. 12. Plots comparing the modeled longwave radiation to that measured inside the trench at four different points. $\downarrow L$ is the incoming longwave radiation measured on a horizontal surface outside the trench. Data corresponds to cloudless days in June.

temperature of the trench walls. While the assumption that the temperature of a shaded wall is equal to the air temperature (on a horizontal surface) is likely to be true in the morning, it is less likely to be so in the midday and afternoon. The wall that was exposed to radiation in the morning and is shaded in the afternoon retains its energy so that the wall surface temperature is likely higher than the air temperature. largest errors occur around noon (Fig. 13), but even at these times the magnitude of the errors is relatively small.

4.3. Sensitivity analysis

To assess the robustness of the model, a sensitivity analysis was conducted on the shortwave radiation model for the following parameters: canopy radius and extinction coefficient. In each case, we ran the model using the geographical coordinates of BIDR, assumed an albedo of 0.35, and simulated two trees spaced 5.0 m apart. Canopy height was adjusted according to the trench's depth and the canopy radius, such that, for cases when the canopy radius was larger than 0.5 m, the gap between the top of the trench and the base of the canopy was always 0.2 m. For cases when the canopy radius was 0.5 m or less, the canopy height was equal to that used for trees with a canopy radius of 0.75 m. For each simulation, a mean value of $\downarrow SR$ inside the TMC was calculated by averaging the value for a grid of points spaced 0.1 m widthwise and 0.25 m lengthwise in the region between the two trees.

To examine the effects of incremental changes in each of the selected variables, we numerically computed the ratio of the relative change in the model's output ($\Delta\downarrow SR$) and the relative change in the input variable (ΔI), following the method described by Oyarzun et al. (2007):

$$\text{Sensitivity}=\frac{\Delta \downarrow SR}{\Delta I} = \frac{(\downarrow SR_1 - \downarrow SR_0)/\downarrow SR_0}{(I_1 - I_0)/I_0} \quad (48)$$

where the subscript "0" denotes the initial value and the subscript "1" denotes the value after an incremental change. For each case, the incremental change was a 10% increase in the input variable. When the value was negative, this indicated that an increase in ΔI led to a decrease in the $\downarrow SR$ inside the trench. These calculations were done using the direct and diffuse input radiations for both cloudless summer (June 2015) and cloudless winter (December 2015) days. $\downarrow SR_0$ and $\downarrow SR_1$ are then the integrated total of the incoming shortwave radiation reaching the floor of a TMC on the respective winter and summer days.

The model's sensitivity to changes in the extinction coefficient were examined for seven different extinction coefficients (0.05, 0.1, 0.25, 0.5, 0.75, 1.0, 1.5 m^{-1}), with four different canopy radii (0.1, 0.5, 1.0, and 1.5 m), two different widths (0.5 and 1.0 m), two different depths (0.5 and 1.0 m), and two different orientations (N-S and E-W). The model's sensitivity to changes in canopy radius was examined for six different radii (0.1, 0.5, 0.75, 1.0, 1.25, and 1.5 m), with five different extinction coefficients (0.1, 0.25, 0.5, 1.0, 1.5 m^{-1}), two different

Table 5
Table comparing the measured and modeled daily totals for incoming longwave radiation inside the trench system. All results are based on 1-hour time-averaged measured and modeled values. Data corresponds to cloudless days in June.

Point	Measured	Modeled	Abs. Diff.	Error	Linear Regression				
	MJ m^{-2} d^{-1}	MJ m^{-2} d^{-1}	MJ m^{-2} d^{-1}	Percent	Slope	Intercept	R^2	Standard Error (W m^{-2})	MAE (W m^{-2})
1	34.17	34.05	0.12	0.4	0.83	66.7**	0.87	11.661	9.4
2	36.04	36.03	0.01	0.02	0.85	60.9***	0.96	6.973	6.8
3	35.45	35.53	0.08	0.2	*0.999*	1.3	0.93	9.888	7.0
4	35.77	35.28	0.49	1.0	0.75	87.4***	0.97	6.413	9.7

MAE is mean absolute error. * $p < .1$; ** $p < .05$; *** $p < .01$. Slopes not significantly different than one are italicized ($p < .05$).

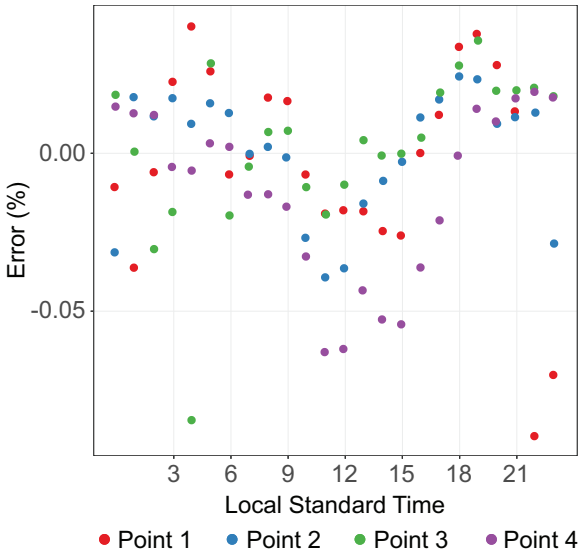

Fig. 13. Plots showing the percent error in the longwave radiation at each of the four points during the validation of the longwave model. Data corresponds to cloudless days in June.

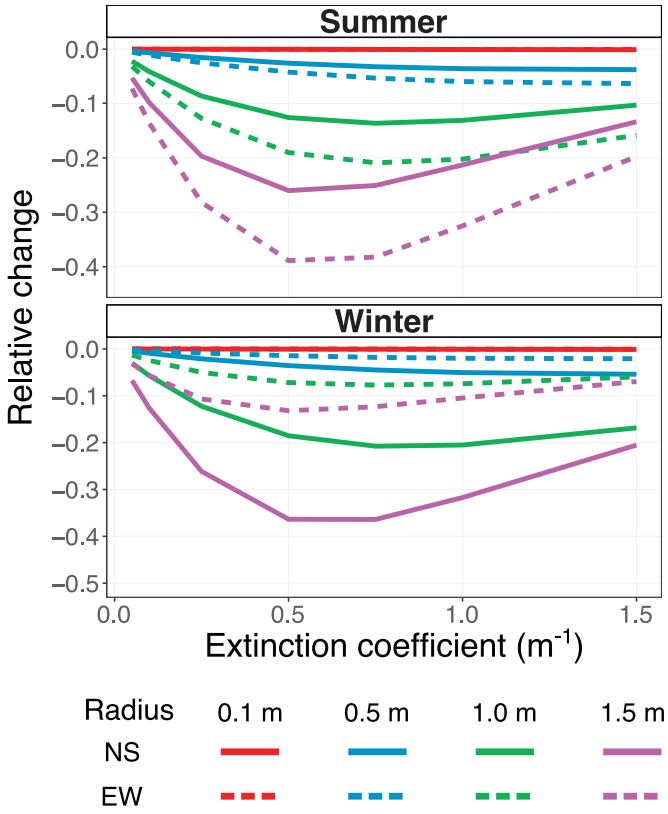

Fig. 14. Plots showing the changes in modeled $\downarrow SR$ reaching the TMC for incremental changes in the extinction coefficient.

widths (0.5 and 1.0 m), two different depths (0.5 and 1.0 m), and two different orientations (N-S and E-W).

The results for the case with a 1.0 m wide and 1.0 m deep TMC are shown in Fig. 14 for the various extinction coefficients and in Fig. 15 for canopy radius. The results from the other configurations are not shown, but were nearly identical.

The results show that the model is considerably more robust to errors in the extinction coefficient than to errors in canopy radius. The maximum sensitivity (absolute value) in the former was less than 0.45, while in the latter it was nearly 3.0. This is because increases in the canopy radius not only result in a larger portion of the trench floor being shaded, but also increases to the canopy depth that radiation must pass through for already shaded points, and therefore more attenuation of the radiation passing through the canopy.

The model's sensitivity to canopy radius increased consistently for both increases in canopy radius and extinction coefficient. In contrast, for cases when the canopy radius was 1.0 m or larger, we observed a maximum sensitivity to extinction coefficient when the extinction coefficient was around 0.5 m^{-1}. As the extinction coefficient increased beyond this level, the model's sensitivity declined. This can be explained by the interaction between the canopy radius and the extinction coefficient. For larger canopy radii, an extinction coefficient greater than 0.5 can result in a canopy that is effectively opaque to incoming shortwave radiation. As the extinction coefficient increases beyond a certain threshold point, incremental increases do not lead to significantly more radiation passing through the canopy. For smaller canopy radii, however, even larger extinction coefficients correspond to a somewhat transparent canopy. The sensitivity to extinction coefficient for simulations with smaller canopy radii therefore continually increases with extinction coefficient.

Orientation and season also have clear effects on the model's sensitivity. In summer, the E-W trenches are most sensitive, while in winter the N-S trenches are most sensitive. This can be explained by considering the shading patterns inside TMCs located at Sede Boqer. In winter, because the sun passes exclusively to the south, any shading produced by the canopy is likely to be projected outside the E-W trenches (i.e., beyond their northern wall). Likewise, the southern wall of E-W trenches produces significant shading during the winter months. Canopy shading therefore does not significantly affect the direct radiation reaching the inside of the trench. In N-S trenches, however, the region just to the north of the trees is inside the trench, and therefore the effects of canopy shading inside these TMCs are more significant. The opposite is true in summer, when changes in the solar elevation and azimuth angles result in canopy shading exerts a stronger influence over conditions inside the E-W oriented TMCs than the N-S TMCs.

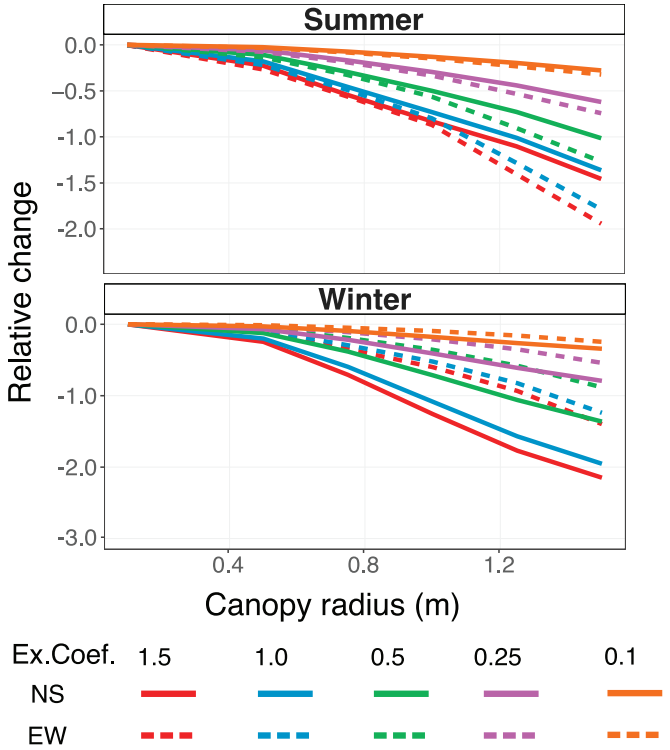

Fig. 15. Plots showing the changes in modeled ↓*SR* radiation reaching the bottom of the trench floor for incremental changes in the canopy radius.

4.4. Simulations

The outputs of the model are the total flux of incoming shortwave and longwave radiation at any number point on the floor of a TMC, at a particular timestep. As such, the model can be used to study radiation distribution patterns within a given trench. We can use the model to understand and assess the effect the presence of a canopy has on both long and short-term trends of incoming all-wave radiation. By using simulations, planners can construct TMCs in a way that minimizes the incoming radiation for a specific site, time of year, and canopy characteristics thereby ensuring maximum amounts of water withn the soil profile.

4.4.1. Effect of changing canopy properties

To demonstrate how the canopy radius and extinction coefficient influence the amount of radiation received by the trench floor, we ran several simulations for TMCs located at BIDR. For each of the simulations, we defined a 5.0 m long focus area, with two identical trees simulated at each end, representing, a typical area between two trees. At each time step, a mean value of the incoming all-wave radiation inside the TMC was determined by calculating the value at each point in a grid (spaced 0.1 m widthwise and 0.50 m lengthwise) and then averaging these values. The simulated trench was 1.0 m wide and 0.75 m deep. As inputs of the diffuse and direct radiation, we used values measured at the BGNSEC.

Fig. 16 shows the fraction of the global shortwave radiation reaching the inside of TMCs with canopy radii of 0.0, 0.5, 0.75, 1.0, 1.25, and 1.5 m. The simulations were run for trenches with both N-S and E-W orientations, using input data from a single cloudless day in both summer and winter. An extinction coefficient of 1.0 m^{-1} was used in all cases.

The simulations show that both orientation and season affect the results. The total radiation reaching the floor of the E-W trenches is greatly reduced with increasing canopy radius during the summer. During the winter, since the trench is shaded most of the time by the walls, the presence of a canopy exerts less influence on the total radiation reaching the floor. The N-S trenches show similar responses to increasing canopy size in both summer and winter, with a slightly greater reduction (in relative terms) in winter.

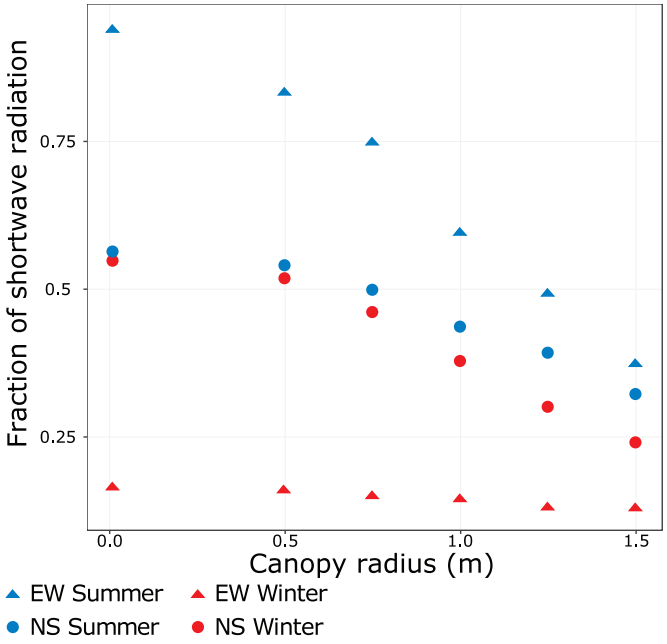

Fig. 16. Fraction of ↓*SR* for simulations run using several different canopy radii. The simulation were run using input data from a single cloudless winter and summer day.

Likewise, we ran similar single-day simulations to examine the effect of the canopy extinction coefficient. For these simulations, we used extinction coefficients of 0.0, 0.5, 1.0, 2.5, 5.0, 7.5 and 10.0 m^{-1}. Trench properties were unchanged from the previous simulations, and the canopy radius was set equal to 1.0 m. Results from the simulations are shown in Fig. 17. As expected, the radiation load on the trench floor decreased with increasing extinction coefficient, except for in the E-W

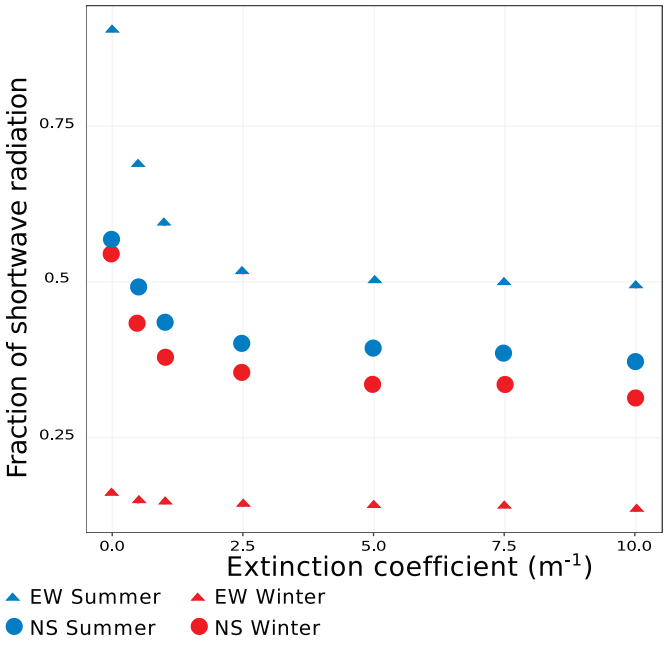

Fig. 17. Fraction of ↓*SR* for simulations run using several different canopy extinction coefficients. The simulations were run using input data from a single cloudless winter and summer day.

orientation in winter, where again, the presence of the canopy has negligible effect.

4.5. Long-term simulations

Agam et al. (2016) showed that orientation exerts a strong effect on the annual patterns of shortwave radiation inside TMCs. Because many arid regions receive rainfall only seasonally, the link between the flux of incoming shortwave radiation and orientation may have important implications. In Sede Boqer, for example, precipitation occurs almost exclusively between November and March. Planners may therefore consider placing more emphasis on minimizing the load of incoming all-wave radiation during the rainy season than during the summer period. While it is clear in Agam et al. (2016) that E-W oriented TMCs at Sede Boqer receive less shortwave radiation in winter, these results did not consider the presence of a canopy.

To explore the effect of a canopy on these results, simulations were run to test the effects of variations in trench width and canopy radius on the total incoming all-wave radiation components reaching the floor of N-S and E-W oriented TMCs in Sede Boqer, using input data from November to March (2015) only. In all cases, the trench depth was held constant at 0.75 m, the canopy height varied such that the gap between the canopy radius and the lip of the trench was consistently 0.2 m, and the other input variables were as noted before.

Fig. 18 shows the total radiation reaching the floor of each of the simulated TMCs. When the canopy radius is 1.0 m, the E-W trenches are always more efficient than the N-S trenches. When the canopy radius is 1.5 m or larger, however, there exists a transition point at which the N-S trenches become more efficient. For a 1.5 m canopy radius, the N-S oriented TMC receives less incoming all-wave radiation than the E-W when the trench width is 1.5 m or greater. For a 2.0 m canopy radius, the N-S oriented TMC receives less radiation than the E-W when the width is 1.0 m or greater.

Because the interaction between canopy radius and trench orientation has the potential to change which orientation of trench is most effective (in comparison to the case when no canopy is present), it will be important for agricultural planners to consider the expected size of the canopy when designing TMC systems. For example, in Sede Boqer, an E-W trench may be more efficient for small trees, while a N-S more efficient for larger trees. Likewise, if there are biological or manpower constraints that govern the width of the trench, this may also affect which orientation is most efficient.

5. Innovation and applications

Our model is unique in its ability to consider the incoming shortwave and longwave radiation inside a trench-shaped micro-catchment, with trees explicitly considered. The most closely comparable models are those used for urban canyons. While several attempts have been made to account for the presence of trees in urban canyon models, these models make fundamental assumptions which are violated in the case of a TMC. Lee and Park (2007) considered a system in which a tree is placed at the center of the canyon, but do not include time step changes in canopy shading. In the case of TMCs, the effect of the canopy on shading patterns is likely to vary considerably with time. Krayenhoff et al. (2013) presented a "multi-layer" model in which trees of any height can be included between and above buildings. The trees inside this model, however, must extend the entirety of the horizontal direction (i.e., the "layer"). Ryu et al. (2015) accounted for the possibility of gaps between trees in the horizontal direction. In each of these cases, however, the constructed model was only two-dimensional, and therefore considered the conditions along the length of the trench to be homogeneous. Trees planted inside a TMC, by contrast, are likely to be spaced with considerable gaps between them, the exact distance dependent on the expected runoff collected at the site and factors such as soil type and slope, which govern the generation of runoff (Critchley and Siegert, 1991). The model proposed by Ryu et al. (2015) is also subject to the additional limitation that the canopy be wholly within the canyon. In the case of TMCs, nearly the entire canopy extends above the height of the canyon walls.

The use of runoff for afforestation, including micro-catchment systems, is increasing, particularly in the less developed areas of drylands (Berliner and Ben-Asher, 1994). Ensuring that the water supply to the trees is adequate is of paramount importance and the TMCs described here have the potential to decrease direct evaporation from the wetted surfaces. The presented model could be used to improve the geometry of the water receiving areas and thus ensure a much higher survival rate of the trees and their development during the early stages. The presented model can provide a tool to planners seeking to minimize evaporative water losses by allowing for the determination of the optimal trench design given constraints such as geographic location, tree properties, and seasonal rainfall patterns.

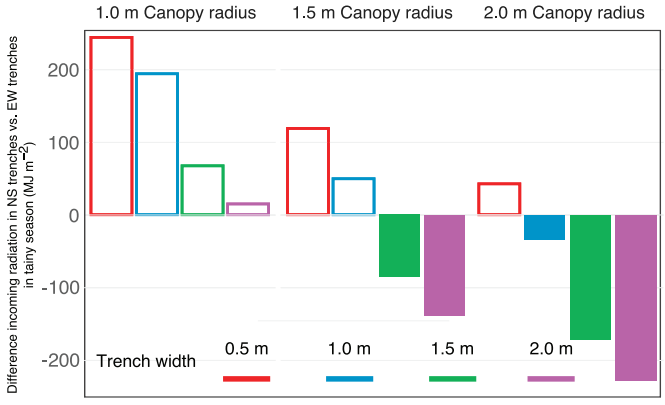

Fig. 18. Plots comparing the incoming shortwave and longwave radiation received by E-W and N-S TMCs during the winter months in Sede Boqer. Solid/negative bars correspond to cases when the N-S oriented trenches received less radiation.

6. Conclusions

The presented model can be used to calculate the incoming shortwave and longwave radiation components at any number of points along the width and length of a TMC, explicitly accounting for the presence of trees. The parameters in the model include location (latitude, longitude, and time zone), trench properties (depth, width, orientation, soil albedo, soil emissivity), tree properties (canopy radius, tree height, canopy opacity, leaf emissivity), direct and diffuse radiation incident on a horizontal surface outside the trench, air temperature, relative humidity, and date and time. In determining the shortwave radiation, the model separately considers the direct, diffuse, and reflected components. For the longwave radiation, the model considers radiation emitted from the atmosphere above the trench, the canopy, and from the trench walls.

Through long-term simulations, the model can contribute to the determination of the optimal configuration of TMCs, for which the incoming all-wave radiation reaching the system is minimized. Because incoming radiation is a prime driver of evaporation, by minimizing the incoming allwave radiation it is expected we will also reduce evaporation, thereby increasing the amount of water available to trees planted in TMCs. The presented model only calculates radiation fluxes, however, and not other factors that influence evaporation, such as wind speed and humidity gradients. We expect, given the presence of a canopy, that the wind speed inside TMCs will be minimal, but additional research is needed to verify this.

Validation of the model showed that it was able to successfully model the diurnal course of shortwave and longwave radiation inside a N-S oriented TMC, at several different points along the trench width

and length and at varying times of year. While overall accuracy was high (maximum error 5%), modeling of the shortwave radiation at points along the boundary of the region shaded by the canopy proved most difficult.

A sensitivity analysis showed that the model was robust to small errors in the measurement of the extinction coefficient, but was noticeably more sensitive to small errors in the canopy radius, especially for simulations with a large canopy radius. In both cases, the model is more sensitive for E-W trenches in summer and in the N-S trenches in winter.

Model simulations show that deeper and narrower TMCs receive less incoming shortwave radiation, but longwave radiation is increased. The reduction in the former is comparatively larger, however, resulting in the ground of TMCs receiving less net incoming all-wave radiation than a horizontal surface outside the trench. Orientation has a considerable effect on the flux of incoming shortwave radiation, influencing the overall performance of a trench. Results show that presence of a canopy inside a TMC can influence the effect of orientation. While E-W trenches were more efficient in winter for the considered simulations when there was no canopy, N-S trenches were in certain cases more efficient when a canopy was included.

Declaration of Competing Interests

None.

Appendix A. Wall shading

The model considers the azimuth (ϕ) and elevation (φ) angles of the sun, the trench's orientation angle with respect to north (*ORI*), and the ratio of the trench's depth (*D*, m) with respect to its width (*W*, m).

At any given time, only one of the trench's walls can produce shade. To determine which wall might shade the floor, we define WALL 1 as the eastern wall of a north-south oriented trench and WALL 2 as the western wall. In an east-west trench, we define WALL 1 as the southern wall. The sun's azimuth angle then determines which of the walls can potentially shade the trench floor (Fig. A.1):

- If $ORI < \phi < ORI + \pi$, shading can be caused by WALL 1
- If $ORI + \pi < \phi < ORI + 2\pi$, shading can be caused by WALL 2

A point, *m*, on the trench floor will be shaded if the length of the shade normal to the trench orientation (*L′*), is greater than the distance from *m* to the trench wall. An example of this is shown in Fig. A.2.

In this case, shading comes from WALL 1. Point m_1 is shaded, while point m_2 is not.

- When $ORI < \phi < ORI + \pi$, m will be shaded if $m > W - L'$
- When $ORI + \pi < \phi < ORI + 2\pi$, m is shaded if $m < L'$

The length of the shade normal to the trench orientation (as detailed in Fig. A.3) is given by:

$$L' = \frac{D}{\tan(\varphi')} \tag{A.1}$$

where:

$$\tan(\varphi') = \frac{\tan(\varphi)}{|\cos(\theta)|} \tag{A.2}$$

and

$$\theta = |\phi - NOR| = |\phi - ORI + \frac{\pi}{2}| \tag{A.3}$$

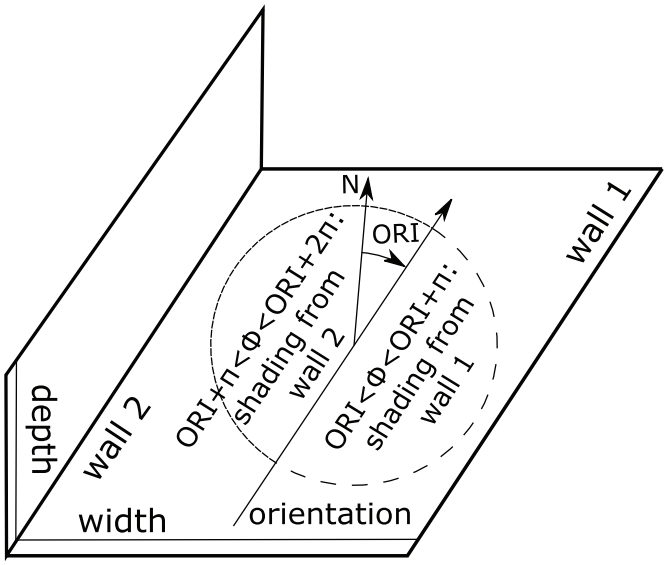

Fig. A1. The azimuth angle of the sun determines which of a TMC's walls can potentially produce shading.

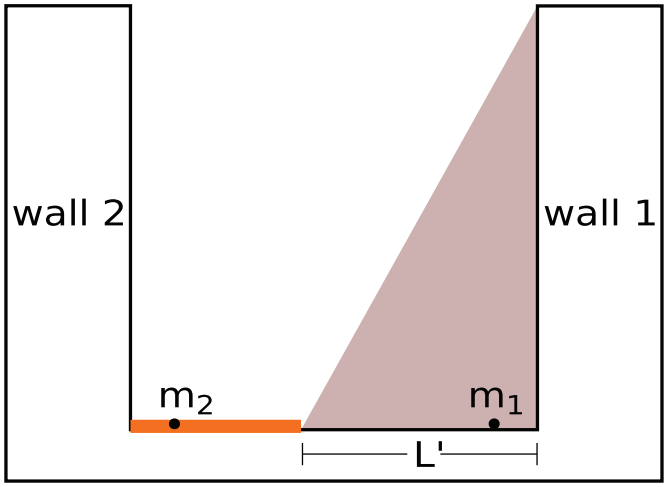

Fig. A2. The length of the shade produced by the TMC's walls (L') determines if a given point on the ground is shaded.

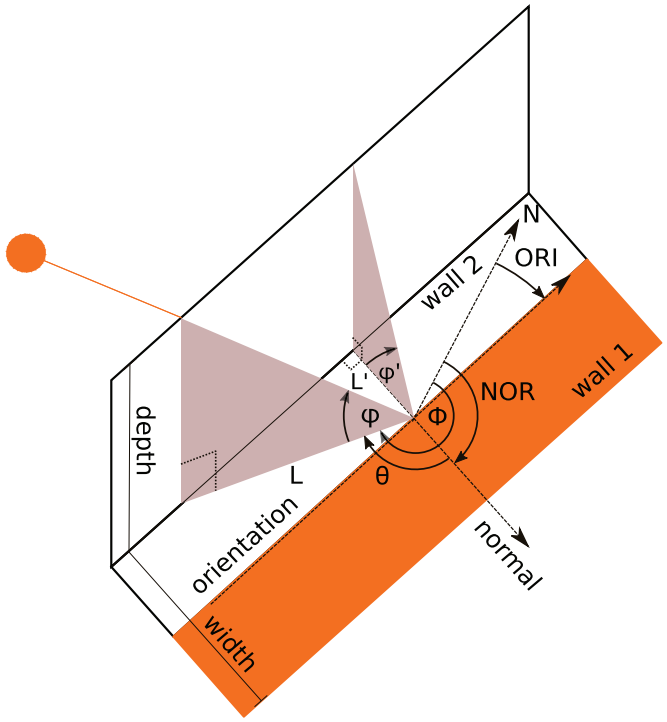

Fig. A3. Demonstration of the calculation of L', the length of the shade produced by the trench's walls, normal to the trench's orientation.

where NOR is the trench orientation with respect to normal:

$$NOR = ORI + \frac{\pi}{2} \tag{A.4}$$

and θ is the angle between ϕ and NOR:

$$\cos\theta = \frac{L}{L'} \tag{A.5}$$

Appendix B. Reflected direct radiation

The reflected direct radiation is dependent on the intensity of the direct radiation reaching the trench's walls (S_W), the height of the illuminated portion of the trench wall (h_{ref}), the wall's albedo (ρ), and the fraction of the reflected direct radiation seen by point m on the trench floor (f_{DIR}). The relationship is defined such that the direct radiation reflected from the trench wall and reaching a point m on the trench floor (S_R) is given by:

$$S_R = \rho S_W f_{DIR} \tag{B.1}$$

In the case where no radiation is attenuated by the canopy, we can use Lambert's Cosine Law to find the intensity of the solar radiation measured

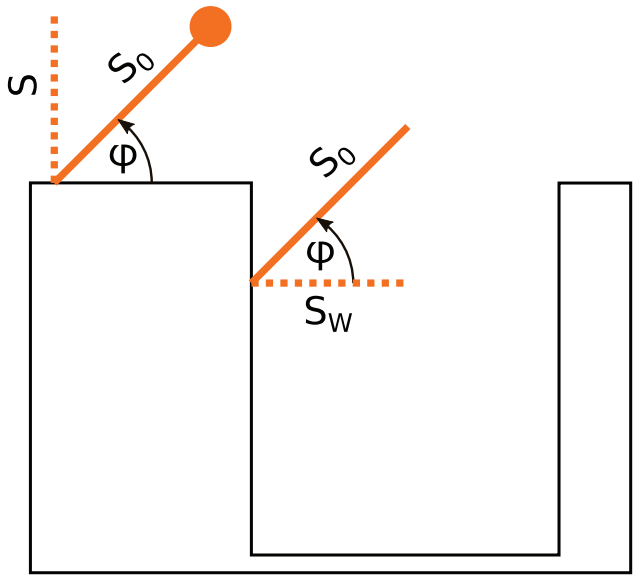

Fig. B4. Demonstration of the calculation of the direct beam radiation reaching a vertical surface, in this case the trench wall.

on the trench wall (S_W):

$$S_W = S\sin(\frac{\pi}{2} - \varphi) = S\cos\varphi \tag{B.2}$$

and where S is the intensity of the solar beam and can be calculated based on S_0, the measured direct radiation outside the trench:

$$S = \frac{S_0}{\sin\varphi} \tag{B.3}$$

The depth to which the wall is illuminated (h_{ref}) depends on the sun's position relative to the trench and the trench's depth to width ratio, such that:

$$h_{ref} = W\tan\varphi' \tag{B.4}$$

The fraction of the reflected radiation seen from point m (f_{DIR}) is dependent on the meridional view angles, as was the case when looking at the diffuse radiation reaching the trench floor. The meridional angles are defined such that:

- when $ORI < \phi < ORI + \pi$:

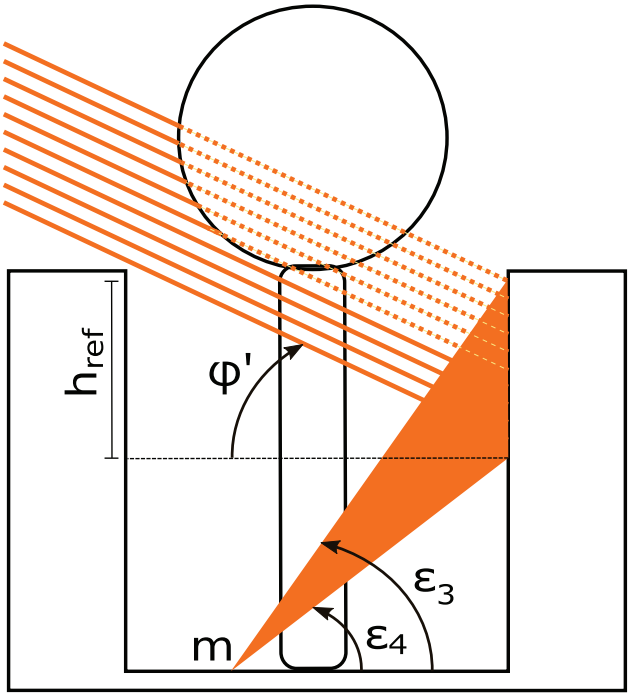

Fig. B5. The meridional angles that determine the fraction of reflected radiation directed from the trench walls to a point m on the floor of a TMC.

$$\varepsilon_3 = \arctan\left(\frac{D}{W - m_x}\right) \tag{B.5}$$

$$\varepsilon_4 = \arctan\left(\frac{D - h_{ref}}{W - m_x}\right) \tag{B.6}$$

- when $ORI + \pi < \phi < ORI + 2\pi$:

$$\varepsilon_3 = \arctan\left(\frac{D}{m_x}\right) \tag{B.7}$$

$$\varepsilon_4 = \arctan\left(\frac{D - h_{ref}}{m_x}\right) \tag{B.8}$$

For the case when there is no canopy within the trench system, the meridional angles can be used in a manner similar to Equation (27) and the fraction of reflected radiation seen from point m can be written:

$$f_{DIR} = \frac{\cos\varepsilon_4 - \cos\varepsilon_3}{2} \tag{B.9}$$

Appendix C. Reflected diffuse radiation

The reflected diffuse radiation is calculated in a manner similar to that of the reflected direct radiation, except that reflected radiation comes from both of the trench walls and the entire height of the wall (not just the illuminated portion).

The reflected diffuse radiation is dependent on the intensity of the diffuse radiation reaching the trench's walls (Ω_W), the wall's albedo (ρ), and the fraction of the reflected diffuse radiation seen by point m on the trench floor (f_{DIF}). The relationship is defined such that the diffuse radiation reflected from the trench wall and reaching a point m on the trench floor (Ω_R) is given by:

$$\Omega_R = \rho\Omega_W f_{DIF} \tag{C.1}$$

For the case when there is no canopy, the diffuse radiation reaching a given point i on the trench wall is dependent on the fraction of the celestial hemisphere seen from that point, as was described in Section 2.1.2.

For point i on the trench wall, we can therefore define the diffuse radiation reaching that point, Ω_{W-i}, such that:

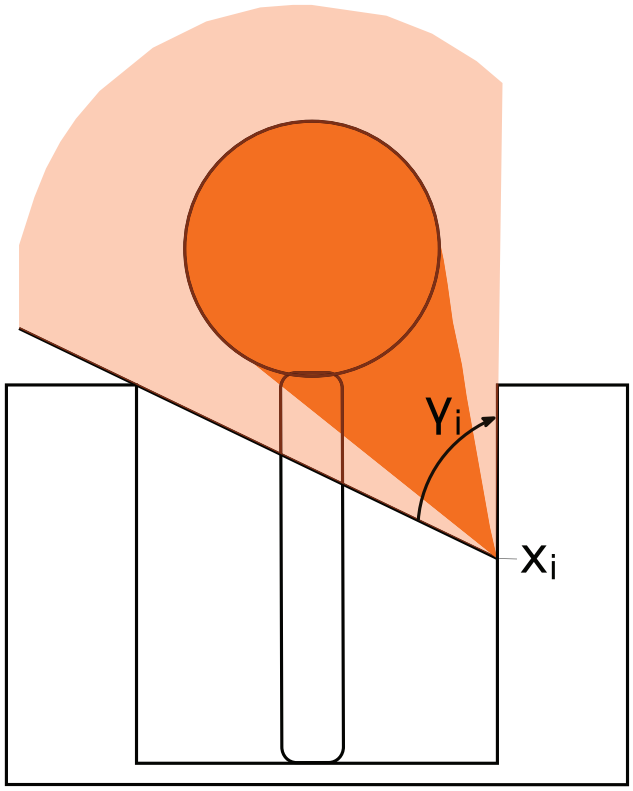

Fig. C6. The fraction of the celestial hemisphere seen from point x_i on the wall of a TMC.

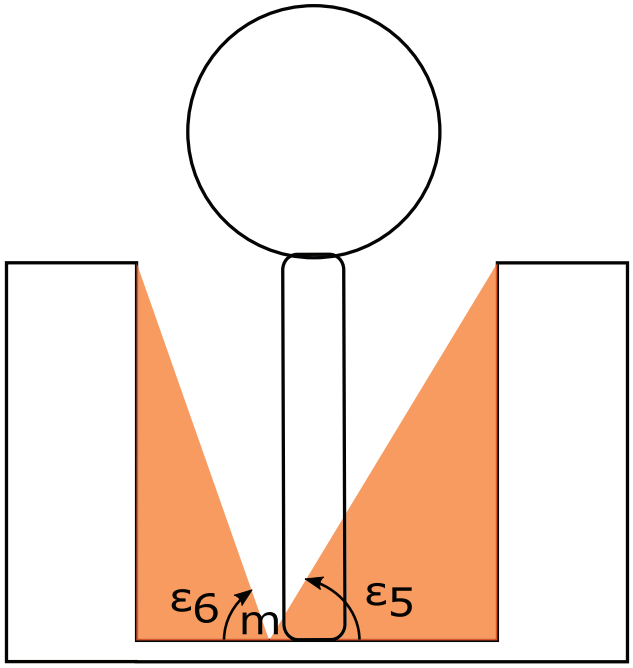

Fig. C7. The fraction of the diffuse radiation reaching the walls of a TMC that is directed towards point *m* on the ground inside a TMC.

$$\Omega_{W-i} = \Omega_a f_i \tag{C.2}$$

where f_i is the fraction of the celestial hemisphere visible from point i and is defined based on the meridional view angles for point i, such that:

$$f_i = 1 - \frac{\cos \gamma_i}{2} \tag{C.3}$$

In this case, γ_i is given by:

$$\gamma_i = \arctan \frac{W}{D - h_i} \tag{C.4}$$

where h_i is the distance from the top of the trench to point i. For points on the wall, the second meridional angle is always equal to zero (Fig. C.6).

An average value of Ω_W could then be found by dividing the trench wall into several intervals and computing Ω_i for each of them. Such that:

$$\Omega_W = \frac{\sum_{i=1}^{n} \Omega_i}{n} \tag{C.5}$$

where n is the number of intervals.

The fraction of Ω_W reaching point m on the bottom of the trench (Fig. C.7) is then dependent on the fraction of the wall visible to point m, which is given by:

$$f_{DIF} = \frac{1 - \cos \varepsilon_5}{2} + \frac{1 - cos\varepsilon_6}{2} = 1 - \frac{(\cos \varepsilon_5 + \cos \varepsilon_6)}{2} \tag{C.6}$$

where ε_5 faces WALL 1 and is given by:

$$\varepsilon_5 = \arctan \frac{D}{m_x} \tag{C.7}$$

and where ε_6 faces WALL 2 and is given by:

$$\varepsilon_6 = \arctan \frac{D}{W - m_x} \tag{C.8}$$

Table 3
The coordinates of each measurement point with respect to the trench's eastern wall (widthwise) and TREE 3 (lengthwise) during the longwave validation.

Point	Width (m)	Length (m)
1	0.45	1.66
2	0.45	0.8
3	0.30	1.02
4	0.30	2.34

References

Agam, N., Leake, S., Berliner, P., 2016. Modeling short wave solar radiation flux in a trench water harvesting system. Agric. For. Meteorol. 221, 152–163. https://doi.org/10.1016/j.agrformet.2016.02.014.

Baldocchi, D.D., Law, B.E., Anthoni, P.M., 2000. On measuring and modeling energy fluxes above the floor of a homogeneous and heterogeneous conifer forest. Agric. For. Meteorol. 102 (2), 187–206. https://doi.org/10.1016/S0168-1923(00)00098-8.

Berliner, P., Ben-Asher, J., 1994. Runoff Irrigation. Springer Berlin Heidelberg, pp. 126–154. https://doi.org/10.1007/978-3-642-78562-7_6. 6

Black, T.A., Chen, J.-M., Lee, X., Sagar, R.M., 1991. Characteristics of shortwave and longwave irradiances under a douglas-fir forest stand. Can. J. For. Res. 21 (7), 1020–1028. https://doi.org/10.1139/x91-140.

Black, T.A., Kelliher, F.M., 1989. Forests, weather and climate - processes controlling understorey evapotranspiration. Philos. Trans. R. Soc. Lond. B: Biol. Sci. 324 (1223), 207–231. https://doi.org/10.1098/rstb.1989.0045.

Boers, T.M., 1994. Rainwater Harvesting in Arid and Semi-Arid Zones. International Land Reclamation and Improvement Institute, Wageningen, The Netherlands.

Brutsaert, W., 2013. Evaporation into the Atmosphere: Theory, History, and Applications. Springer, Netherlands.

Critchley, W., Siegert, K., 1991. A Manual for the Design and Construction of Water Harvesting Schemes for Plant Production. Technical Report. Food and Agriculture Organization of the United Nations, Rome, Italy.

Duursma, R., Marshall, J., Robinson, A., 2003. Leaf area index inferred from solar beam transmission in mixed conifer forests on complex terrain. Agric. For. Meteorol. 118 (3–4), 221–236. https://doi.org/10.1016/S0168-1923(03)00109-6.

Essery, R., Pomeroy, J., Ellis, C., Link, T., 2008. Modelling longwave radiation to snow beneath forest canopies using hemispherical photography or linear regression. Hydrol. Process. 22 (15), 2788–2800. https://doi.org/10.1002/hyp.6930.

Hillel, D., 2003. 20 - water balance and energy balance in the field. In: Hillel, D. (Ed.), Introduction to Environmental Soil Physics (First), First. Academic Press, Burlington, pp. 385–405. https://doi.org/10.1016/B978-012348655-4/50021-6.

IPCC, 2007. Climate Change 2007: Synthesis Report. Contribution of Working Groups I, II and III to the Fourth Assessment Report of the Intergovernmental Panel on Climate Change. Technical Report. Geneva.

Jiang, A., 2016. Effect of soil type and surface layer on non-rainfall water inputs. Ben-Gurion University of the Negev.

Jonckheere, I., Fleck, S., Nackaerts, K., Muys, B., Coppin, P., Weiss, M., Baret, F., 2004. Review of methods for in situ leaf area index determination. Agric. For. Meteorol. 121 (1–2), 19–35. https://doi.org/10.1016/j.agrformet.2003.08.027.

Krayenhoff, E.S., Christen, A., Martilli, A., Oke, T.R., 2013. A multi-layer radiation model for urban neighbourhoods with trees. Bound. Layer Meteorol. 151 (1), 139–178. https://doi.org/10.1007/s10546-013-9883-1.

Leake, S., 2015. The efficiency of trenches as runoff water harvesting systems and the role of their design in minimizing water losses. Ben-Gurion University of the Negev Mathesis.

Lee, S., Park, S., 2007. A vegetated urban canopy model for meteorological and environmental modelling. Bound. Layer Meteorol. 126 (1), 73–102. https://doi.org/10.1007/s10546-007-9221-6.

Lu, H., Wei, W.-s., Liu, M.-z., Han, X., Hong, W., 2014. Observations and modeling of incoming longwave radiation to snow beneath forest canopies in the west tianshan mountains, china. J. Mt. Sci. 11 (5), 1138–1153. https://doi.org/10.1007/s11629-013-2868-1.

Macfarlane, C., Arndt, S.K., Livesley, S.J., Edgar, A.C., White, D.A., Adams, M.A., Eamus, D., 2007. Estimation of leaf area index in eucalypt forest with vertical foliage, using cover and fullframe fisheye photography. For. Ecol. Manage. 242 (2), 756–763. https://doi.org/10.1016/j.foreco.2007.02.021.

Nyman, P., Metzen, D., Hawthorne, S.N., Duff, T.J., Inbar, A., Lane, P.N., Sheridan, G.J., 2017. Evaluating models of shortwave radiation below eucalyptus canopies in se australia. Agric. For. Meteorol. 246, 51–63. https://doi.org/10.1016/j.agrformet.2017.05.025.

Oke, T.R., 2002. Boundary Layer Climates. Routledge.

Oyarzun, R.A., Stöckle, C.O., Whiting, M.D., 2007. A simple approach to modeling radiation interception by fruit-tree orchards. Agric. For. Meteorol. 142 (1), 12–24. https://doi.org/10.1016/j.agrformet.2006.10.004.

Pomeroy, J.W., Marks, D., Link, T., Ellis, C., Hardy, J., Rowlands, A., Granger, R., 2009. The impact of coniferous forest temperature on incoming longwave radiation to melting snow. Hydrol. Process. 23 (17), 2513–2525. https://doi.org/10.1002/hyp.7325.

Rutten, Y., 2008. Pan evaporation from trenches with different geographical alignment and depth: width ratios. Ben-Gurion University of the Negev mathesis.

Ryu, Y., Bou-Zeid, E., Wang, Z., Smith, J.A., 2015. Realistic representation of trees in an urban canopy model. Bound. Layer Meteorol. 159 (2), 193–220. https://doi.org/10.1007/s10546-015-0120-y.

Saitoh, T.M., Nagai, S., Noda, H.M., Muraoka, H., Nasahara, K.N., 2012. Examination of the extinction coefficient in the beer–lambert law for an accurate estimation of the forest canopy leaf area index. Forest. Sci. Technol. 8 (2), 67–76. https://doi.org/10.1080/21580103.2012.673744.

Silberstein, R., Held, A., Hatton, T., Viney, N., Sivapalan, M., 2001. Energy balance of a natural jarrah (eucalyptus marginata) forest in western Australia: measurements during the spring and summer. Agric. For. Meteorol. 109 (2), 79–104. https://doi.org/10.1016/S0168-1923(01)00263-5.

Zhang, S., Carmi, G., Berliner, P., 2013. Efficiency of rainwater harvesting of micro-catchments and the role of their design. J. Arid Environ. 95, 22–29.

Zhao, W., Qualls, R., Berliner, P., 2003. Modeling of the short wave radiation distribution in an agroforestry system. Agric. For. Meteorol. 118 (3–4), 185–206. https://doi.org/10.1016/S0168-1923(03)00108-4.